Electronic Supplementary Material (ESI) for Chemical Science.

Supporting information for:

C-terminal truncation of α-synuclein promotes amyloid fibril amplification at physiological pH

Ingrid M. van der Wateren,[†] Tuomas P. J. Knowles,[†,‡] Alexander K. Buell,[*,¶] Christopher M. Dobson,[*,†] and Céline Galvagnion[*,§]

†*Department of Chemistry, University of Cambridge, Lensfield Road, Cambridge CB2 1EW, United Kingdom*

‡*Cavendish Laboratory, Department of Physics, University of Cambridge, J J Thomson Avenue, Cambridge, CB3 1HE, United Kingdom*

¶*Institute of Physical Biology, Heinrich Heine Universität, Universitätsstr.1, 40225, Düsseldorf, Germany*

§*Present address: German Center for Neurodegenerative Diseases (DZNE), Sigmund-Freud-Str. 27, 53127, Bonn, Germany*

E-mail: Alexander.Buell@uni-duesseldorf.de; cmd44@cam.ac.uk; celine.galvagnion@dzne.de

Supplementary Methods

Protein expression and purification

AS(WT) and AS(1-119) were purified using the same protocol as that described previously.[S1,S2] In particular, competent cells (OneShot BL21 (DE3) (gold), Invitrogen) were transformed with a PT7-7 plasmid carrying the gene for the protein of interest. 1 ml LB medium (MP bio) was added and cells placed in a 37 °C incubator for 45 minutes. Cells were plated on ampicillin (Sigma-Aldrich) containing LB agar plates and incubated at 37 °C overnight. The next morning, a single culture was transferred to 5-50 ml of ampicillin containing LB medium and left to incubate whilst shaking at 37 °C for ca. 8 hours. 2.5-5 ml of culture were transferred to 0.5 L of OverNight Express Instant TB medium (EMD Millipore) supplemented with ampicillin and left to incubate at 30 °C for 18-24 hours shaking at 180 rpm. Cells were collected by centrifugation at 5 krpm for 45 minutes at 4-8 °C using a Beckman Coulter Avanti J-20 XPI centrifuge. The supernatant was poured off and the pellets resuspended in 1X PBS (Oxoid Limited) using 25 ml per 0.5 L original culture. This solution was placed in 50 ml tubes and centrifuged at 4 krpm for 1 hour at 4 °C using a benchtop centrifuge (Thermo Scientific, Heraeus Multifuge X3R). The supernatant was poured off and the pellets transferred to -80 °C for storage. For purification, the pellets were resuspended in 10 mM Tris pH 8.0 (Sigma) with 1 mM EDTA (Sigma) and a protease inhibitor (cOmplete^{TM} EDTA-free protease inhibitor cocktail tablets, Sigma-Aldrich). The solutions were pooled into a beaker and sonicated at level 7 for 5 minutes total ON-time, with 15 s. ON, 45 s. OFF cycle (Ultrasonic processor XL, Misonix Incorporated). This cell lysate was centrifuged for 20 minutes at 13.5 krpm, 4 °C using a Beckman Coulter Avanti J-20 XPI centrifuge, which was used for the subsequent centrifugation steps. The supernatant was transferred to new tubes and incubated for 20 minutes in a 85-90 °C water bath followed by centrifugation at 13.5 krpm for 20 minutes at 4 °C: the supernatant was retained. Streptomycin sulfate (Sigma) was added to this supernatant at 10 mg/ml and left to incubate at 10

°C for 15 minutes on a rotating bed, after which the solution was centrifuged at 13.5 krpm for 20 minutes at 4 °C, the supernatant taken and this step repeated. Ammonium sulfate (Fischer Scientific) was added at 360 mg/ml and the solution was left to incubate at 10 °C for 30 minutes on a rotating bed. The solutions was centrifuged at 13.5 krpm for 20 minutes at 4 °C and the supernatant was discarded. The pellets were resuspended in 25 mM Tris pH 7.7 (Sigma) and the solutions left to dialyse over night in the same buffer using 2 L buffer, which was replaced once. After dialysis, anion-exchange chromatography (HiLoad^{TM} 26/10 SP Q sepharose high performance, GE Healthcare) was performed using 25 mM Tris pH 7.7 (Sigma), and this same buffer with addition of 1-1.5 M NaCl (VWR Prolabo) for elution. Fractions were loaded on a NuPage 4-12% Bis-Tris gel (Invitrogen) to inspect composition of fractions using SeeBlue Plus2 pre-stained protein standard (Invitrogen). Fractions containing protein of interest were pooled and concentrated for size exclusion chromatography (HiLoad^{TM} Superdex^{TM} 75 prep grade 26/600, GE Healthcare) which was performed using 20 mM sodium phosphate buffer (NaH_2PO_4/Na_2HPO_4, 0.01% NaN_3) pH 6.5. A small volume of each SEC fraction was loaded on a 4-12% Bis-Tris gel to inspect purity of fractions. Fractions were pooled and concentrated, then divided into small aliquots (0.25-1 ml, or 5-10 ml) which were snap-frozen in liquid nitrogen and stored at -80 °C. Mass-Spectrometry was performed to determine the molecular weights of the purified proteins (Protein & Nucleic Acid Chemistry facility, Department of Biochemistry, University of Cambridge, UK).

AS(1-103) was expressed and purified in the same way as AS(WT) and AS(1-119) except that the plasmid for AS(1-103) encodes for kanamycin resistance instead of ampicillin resistance. Kanamycin (Sigma-Aldrich) stock solution was 15-30 mg/ml which was diluted 1 to 1000 for final use. The purification of AS(1-103) was different from that of AS(WT) and AS(1-119) with respect to the anion-exchange step: due to the pI of AS(1-103), cation-exchange chromatography was more appropriate. We used two 5 ml HiTrapSP HP (GE Healthcare) columns in sequence and 25 mM MES pH 6.0 (Sigma), instead of 25 mM Tris pH 7.7, and 25 mM MES pH 6.0 with 1.5 M NaCl for elution.

When a different buffer was required for the protein solution, the protein was dialysed against the buffer of interest using a dialysis membrane (SpectraPor 3.5 kDa dialysis tube, Spectrum Labs) in 2 L buffer (twice) at 10 °C. After purification and/or dialysis, the concentration of protein in the solution was determined using absorbance at 278 nm (Cary400 UV-Vis (Varian) or CLARIOstar (BMG LabTech)) using an extinction coefficient of 5600 $M^{-1}.cm^{-1}$ for AS(WT) and 1400 $M^{-1}.cm^{-1}$ for AS(1-119) and AS(1-103) (determined using the Scripps protein calculator at *http://protcalc.sourceforge.net*), correcting for the buffer signal. The protein solution was then divided into small aliquots, which were snap-frozen in liquid nitrogen and stored at -80 °C.

Production of seed fibrils

The protocol of seed fibril production described in the Experimental section of the main manuscript involved incubation of 260 μM monomeric protein at 45°C and strong stirring and in addition sonication for 10 s after 24, 48 and 50 h (Protocol 2). In order to test whether the intermediate and final sonication steps had an effect on the degree of conversion of the soluble protein into fibrils, we also prepared fibrils without any sonication (Protocol 1) or with 1 min of sonication at 24, 48 and 50 h (Protocol 3). At 50 h, we centrifuged the samples and measured the concentration of protein in the supernatant. We found the following concentrations (in μM) of soluble protein in the supernatant at the end of different protocols:

Protocol	[AS(WT)]	[AS(1-119)]	[AS(1-103)]
1	10.0	10.7	25.7
2	10.9	6.4	16.4
3	11.1	7.1	17.9

These results suggest that for the truncated variants, the sonication has a small beneficial effect on the degree of conversion. It is interesting to note that in the AS(WT) sample, 10 μM of soluble protein were found, corresponding to a concentration much higher than the lowest concentration at which fibril growth can still be measured (1 μM,[S3]), suggesting that the

samples prepared at such high protein concentrations do not reach complete thermodynamic equilibrium. However, the percentage of unconverted monomer is relatively small (<10% in all cases) and therefore the error induced from adding some monomer with the seed fibrils in seeded experiments is negligible.

Analysis of seeded aggregation kinetics with AS(WT) seeds

We determined the fibril elongation rate by converting the fluorescence intensity data in Figure 2a (left column) in units of fibril mass concentration, by measuring the quantity of soluble protein left at the plateau phase.[S4] The overall ThT quantum yield is plotted as a function of the concentration of insoluble protein in Figure S4. We find that in all cases, the fluorescence yield is a decreasing function of the total concentration of insoluble protein. In the case of AS(WT) seeds elongated with AS(WT) protein, the quantum yield is weakly decreasing, whereas it decreases more strongly when AS(WT) fibrils were used to seed AS Ctt protein. We used linear fits of the early times of the seeded aggregation time courses ($\sim$ first hour) to obtain the absolute rate of aggregate formation. The early times were chosen for the analysis, because processes other than fibril elongation, such as higher order assembly of the fibrils, but also depletion of ThT are least relevant, while the monomer concentration corresponds approximately to the initial concentration, simplifying the analysis.[S5] Given that in the first hour, up to 50 μM protein was converted into fibrils, we used an average ThT quantum yield of 1000 a.u./μM of insoluble protein (see Figure S4a) in all cases for the conversion into absolute rates of fibril mass increase. We then plotted the initial elongation rate, r, as a function of the monomer concentration, $[m]$, (see Figure 2c) and fitted this data to an equation of the form:[S5,S6]

$$r([m]) = \frac{r_{\max}[m]}{[m] + [m]_{1/2}} \tag{1}$$

where $[m]_{1/2}$ corresponds to the monomer concentration at which half of the maximal rate is reached (see Figure 2c, dotted lines, r_{max} = 5.43 ± 0.72 (AS(WT)), 2.50 ± 0.25 (AS(1-119)) and 1.90 ± 0.10 (AS(1-103)) x 10^{-9} M.s^{-1}; $m_{1/2}$ = 24.8 ± 11.0 (AS(WT)), 10.0 ± 4.9 (AS(1-119)) and 10.3 ± 2.6 (AS(1-103)) μM). We have previously given a detailed discussion of the origin of the saturation behaviour of the fibril growth rate with increasing monomer concentration.[S6] Briefly, this behaviour is due to the finite time that a protein monomer spends at the end of a fibril before it incorporates into the latter, upon which a new monomer can attach. This leads to a finite maximal rate of monomer incorporation. In the limit of low monomer concentrations, this expression reduces to:

$$\lim_{m\to 0} r([m]) = \frac{r_{\max}}{[m]_{1/2}}[m] = k_+[P][m] \tag{2}$$

Therefore, the absolute elongation rate can either be determined from a fit to the full, saturated curve (see Figure 2c, dotted lines), which yields both $r_{\max}$ and $[m]_{1/2}$, or else from a linear fit to the elongation rate data at low monomer concentration (see Figure 2c, solid lines), which yields the ratio $\frac{r_{\max}}{[m]_{1/2}}$. However, in both cases, the concentration of fibril ends, $[P]$, is also required. In order to obtain an estimate of $[P]$, we determined the length distribution of the WT seed fibrils (see histogram in Figure S3). We find an average fibril length of 154 nm, which, together with an average fibril thickness of 7±2 nm (also from AFM imaging), we can calculate an average number of monomers per seed fibril of ∼330 (ρ_{AS} = 1.35 g/cm^3, M_{AS} = 14.5 kDa). For a mass concentration of added seeds of 5 μM, this corresponds to a value of $[P]$ of 30 nM, assuming that elongation occurs from both ends. This value of $[P]$ was used to compute the elongation rate constants, k_+. When using the full fit (see Figure 2c, dotted lines), we obtain rate constants of 7258 M^{-1}s^{-1} for AS(WT), 8333 M^{-1}s^{-1} for AS(1-119) and 6090 M^{-1}s^{-1} for AS(1-103), whereas if we use a linear fit of the data points at low concentration (see Figure 2c, solid lines), we obtain rate constants of 3616 M^{-1}s^{-1} for AS(WT), 2779 M^{-1}s^{-1} for AS(1-119) and 1963 M^{-1}s^{-1} for AS(1-103).

Considering the low quality of the fits to the full saturation curves, as well as the previously determined value for AS(WT) monomers adding onto AS(WT) seeds[S5] ($\sim$2200 $M^{-1}s^{-1}$), we believe that the linear fit to the low concentration data is more reliable.

Analysis of lipid-induced aggregation kinetics of AS(WT) and AS(1-119)

We analysed the kinetic traces corresponding to the lipid-induced aggregation of AS(WT) and AS(1-119) by converting the fluorescence intensity data in Figure S12a and 6a in units of fibril mass concentration, by measuring the quantity of soluble protein left at the plateau phase.[S4] We fitted the early times of the lipid-induced aggregation time courses using the model described previously[S4] and the following equation:

$$M(t) = \frac{K_M k_+ m(0)^{n+1} k_n b t^2}{2(K_M + m(0))} \tag{3}$$

where k_+ is the elongation rate constant of fibrils from lipid vesicles, k_n is the heterogeneous primary nucleation rate constant, n is the reaction order of the heterogeneous primary nucleation reaction relative to the free monomer, m, (n fixed to 0.2, as determined previously[S4]), b is the total mass concentration of the protein bound to the lipid at 100% coverage ($b = \frac{[\mathrm{DMPS}]}{L}$, with L the stoichiometry) and K_M is the Michaelis constant (fixed at 125 μM, as determined previously[S4]). This global analysis yields $k_n k_+$ for each variant (Figure S12b,c).

Supplementary Results

Notes on the pH dependencies

The biggest impact of substantial C-terminal truncation of AS is, besides the obvious change in size, the dramatic change in charge properties. Given the strong influence of truncation on fibril growth and higher order association of fibrils, we decided to systematically investigate

the effect of pH on the aggregation under a range of different conditions. First, we investigated the effect of pH on the degree of completion of the reaction of *de novo* (unseeded) amyloid formation. For this purpose, we quantified the concentration of soluble protein at the end of the reaction of fibrillation (see Experimental section and Supplementary Methods for details on the protocol used) using absorbance spectroscopy (Figure S7). A high concentration of soluble protein in the presence of fibrils, that remains constant in time can indicate either a low thermodynamic stability of the aggregates under these conditions,[S7,S8] or that the reaction is kinetically trapped and not able to reach thermodynamic equilibrium.[S4] In order to avoid kinetic trapping of the system through burial of fibril ends inside clusters (see discussion in main text), the reactions were carried out under strong mechanical stirring, as well as sonication to fragment the fibril clusters and individual fibrils. We found that between pH 4 and pH 7, the aggregation reaction reached near-quantitative completion in all cases. Outside this range, however, we found that at higher pH values, the WT protein did no longer quantitatively convert into aggregates, whereas at lower pH values, the Ctt variants formed very little aggregates. This result can be rationalised in a similar manner to the pH dependence of higher order assembly presented above: removing the protein too far from its isoelectric point increases its net charge and charge density and will render aggregation less favourable. It is well-established that due to the homopolymeric nature of amyloid fibrils, the kinetics[S9] as well as the thermodynamics[S8] of their formation are strongly influenced by electrostatic effects.

Differential scanning calorimetry

We used DSC to characterise the thermotropic properties of DMPS bound to the AS Ctt variants (Figure S11c). As observed for AS(WT),[S10] the binding of the Ctt variants induced a decrease in the melting temperature, T_m, of the lipids of ~ 15°C (Figure S11c). The T_m of the DMPS bound to AS was found to decrease with the decreasing length of the protein, suggesting that not only the N-terminal region of AS, which is directly bound to the lipids,

influences the lipid properties, but also, though to a lesser extent, the (presence or absence of the) C-terminal region.

Supplementary Tables

Table S1: C-terminal truncation (Ctt) affects AS aggregation *in vitro* and *in vivo*

Ctt AS variant	Effect/behaviour	Ref
1-110, 1-120	Formation of "long regular filaments"	S11
1-130	Formation of "small irregular wavy assemblies"	
1-87, 1-120	Faster aggregation than that of AS(WT)	S12
1-89, 1-102, 1-110, 1-120, 1-130	Faster aggregation than that of AS(WT)	S13
1-120	Non detectable seeding of AS(WT) aggregation	
1-89, 1-102, 1-110	Can seed AS(WT) aggregation	
1-108, 1-124	Ctt AS showed higher aggregation propensity (shorter lag phase, higher rate) dependent on solution conditions	S14
1-119, 1-122, 1-123	Ctt AS observed in brain	S15
1-120, 1-123	Faster aggregation rate than that of AS(WT) Substoichiometric amounts of Ctt induce higher amount of aggregated AS(WT)	
1-110, 1-120	Substoichiometric amounts of Ctt AS promoted aggregation of AS(WT) co-overexpression of Ctt AS with AS(WT) increases SH-SY5Y cell vulnerability to oxidative stress	S16
1-57, 1-73, 1-74, and 1-83	Fragments generated by calpain-mediated cleavage of soluble AS(WT), they did not form fibrils and inhibited AS(WT) fibril formation	S17
1-114, 1-122	Fragments generated by calpain-mediated cleavage of AS fibrils, they remained fibrillar and induced co-assembly of AS(WT) monomers	
1-130	Loss of DA neurons in SNpc of mice expressing AS 1-130 as opposed to mice expressing AS(WT) showing no pathology	S18
1-74	Assembly into thin (4.5 Å) fibrils	S19
1-110	Expression of Ctt AS induces mild-moderate pathology without cell loss Co-expression of Ctt AS with AS(WT) induces more aggressive pathology, including accumulation of AS(WT) and formation of larger aggregates	S20
1-135, 1-133, 1-122, 1-119	Shorter lag-phase and higher fibril yield as a larger proportion of the C-terminus was truncated	S21
1-121	Faster aggregation than that of AS(WT)	S22

Notes: DA neurons: dopaminergic neurons; SNpc: substantia nigra pars compacta

Table S2: Estimated charge of AS(WT), AS(1-119) and AS(1-103) over a pH range from 3.0-9.0 with 0.2 pH unit increments (http://protcalc.sourceforge.net)

pH	AS(WT)	AS(1-119)	AS(1-103)
3.0	15.6	15.9	16.2
3.2	15	15.5	15.8
3.4	14.2	14.9	15.4
3.6	13	14.1	14.9
3.8	11.3	13	14.2
4.0	9.3	11.6	13.3
4.2	6.8	9.9	12.2
4.4	4.0	8.0	11.0
4.6	1.3	6.2	9.9
4.8	-1.2	4.6	8.8
5.0	-3.2	3.2	8.0
5.2	-4.8	2.1	7.3
5.4	-5.9	1.4	6.8
5.6	-6.7	0.8	6.5
5.8	-7.3	0.4	6.2
6.0	-7.7	0.1	6.0
6.2	-8.0	-0.1	5.8
6.4	-8.2	-0.3	5.6
6.6	-8.5	-0.5	5.5
6.8	-8.6	-0.7	5.3
7.0	-8.8	-0.8	5.2
7.2	-9.0	-1.0	5.0
7.4	-9.1	-1.1	4.9
7.6	-9.3	-1.3	4.7
7.8	-9.4	-1.4	4.6
8	-9.7	-1.6	4.4
8.2	-9.9	-1.8	4.2
8.4	-10.2	-2.1	3.9
8.6	-10.5	-2.4	3.6
8.8	-11	-2.8	3.2
9.0	-11.6	-3.4	2.6

Table S3: pH of selected organelles[S23]

organelle	pH	AS(WT)	AS(1-119)	AS(1-103)
Mitochondrion	8	N	N	Y
Nucleus	7.2	N	N	Y
Cytosol	7.2	N	N	Y
ER	7.2	N	N	Y
Peroxisome	7	N	Y	Y
Golgi (cis)	6.7	N	Y	Y
Recycling endosome	6.5	N	Y	Y
Early endosome	6.3	N	Y	Y
Golgi (trans)	6	N	Y	Y
Secretory granules	5.5	Y	Y	-
Late endosome	5.5	Y	Y	-
Lysosome	4.7	Y	Y	N

Notes: Y and N indicate whether or not secondary processes were found to contribute to the aggregation of AS(WT), AS(1-119) or AS(1-103) at the pH value corresponding to that of the organelle.

Supplementary Figures

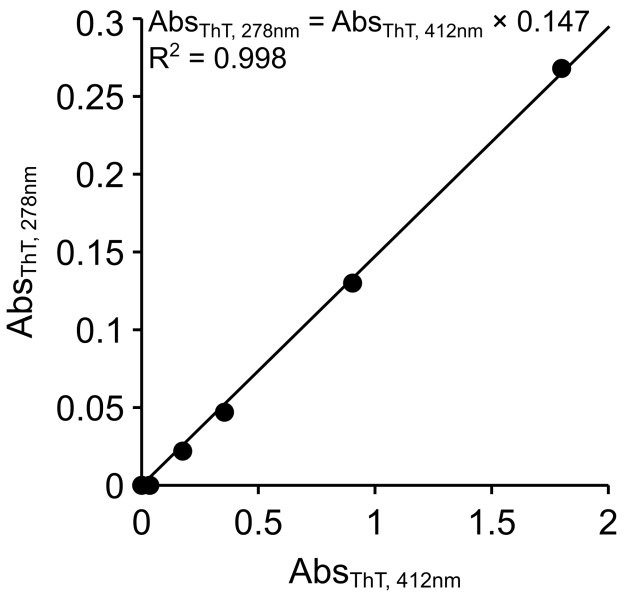

Figure S1: Thioflavin-T absorbance at 278 and 412nm. Change in the absorbance of ThT measured at 278nm as a function of that measured at 412nm.

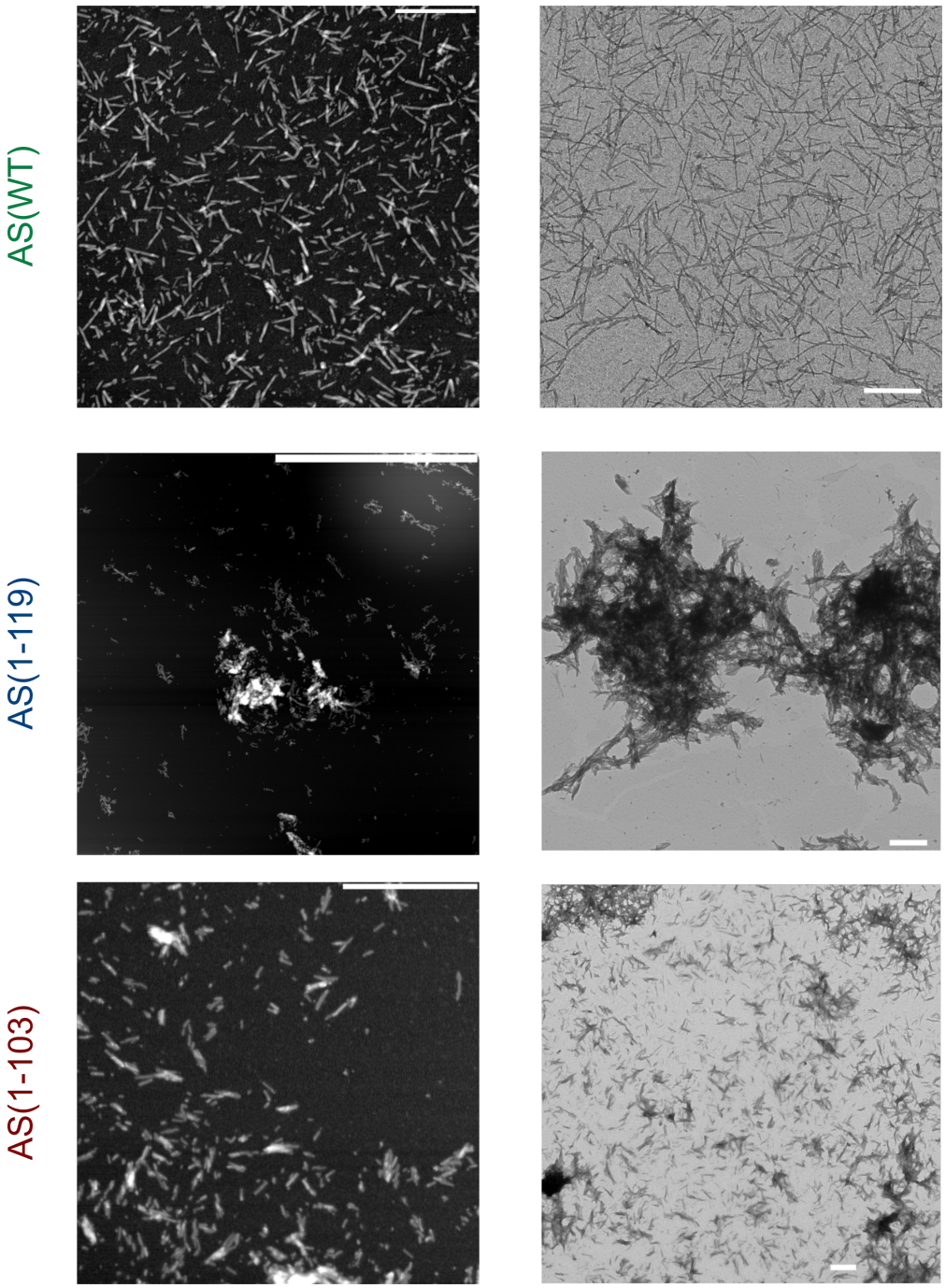

Figure S2: Morphology of seed fibrils made with AS(WT), AS(1-119) and AS(1-103). The scale bars of the AFM images correspond to 1 μm (top and bottom) or 5 μm (middle) and those of TEM images correspond to 500 nm. The AFM slides were prepared using 2 μM fibril solutions and TEM grids were prepared using fibril solutions at the following concentrations: 10 (AS(WT), top), 60 (AS(1-119), middle) and 100 (AS(1-103), bottom) μM. The fibril concentrations are expressed in monomer equivalents.

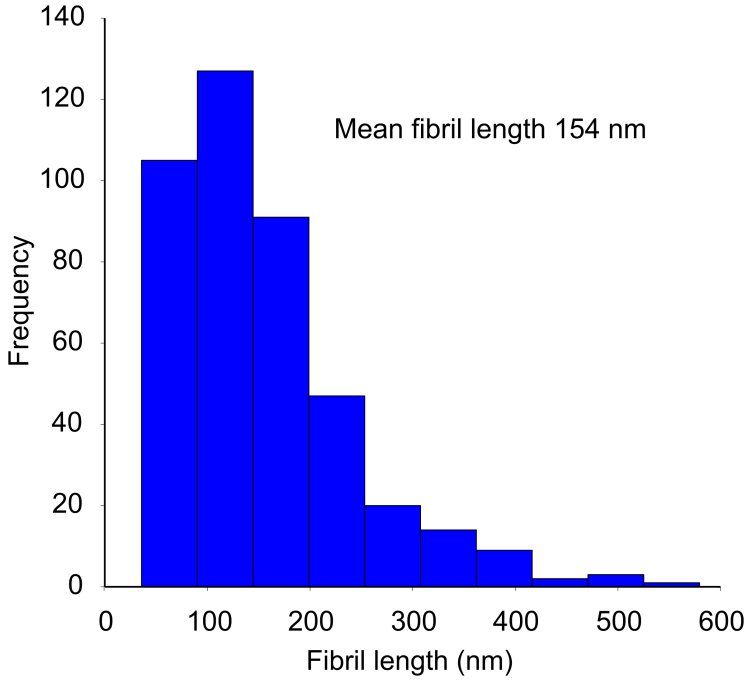

Figure S3: Length distribution of the pre-formed fibril seeds prepared from AS(WT) (see Figure S2).

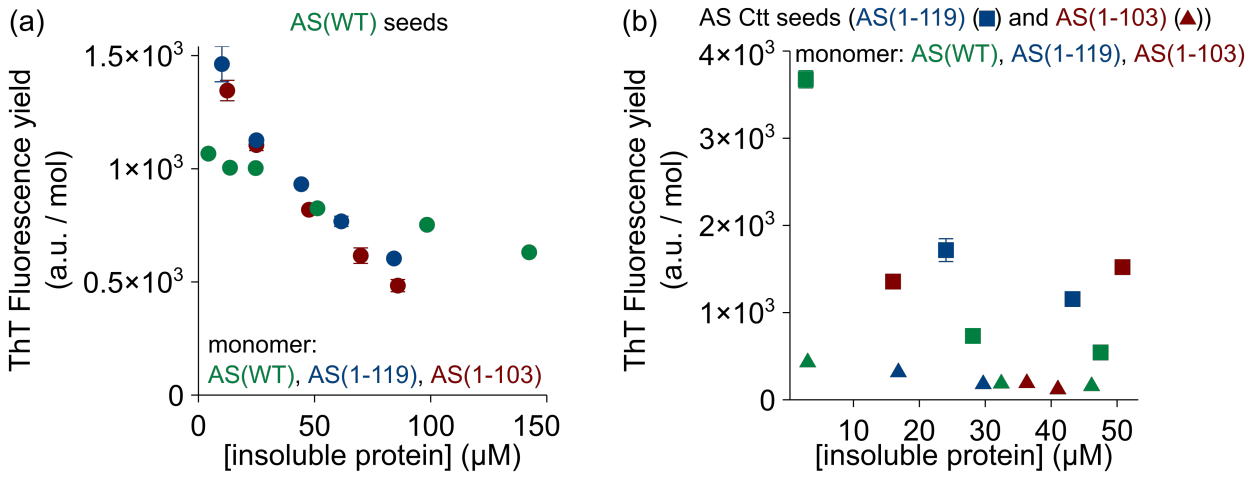

Figure S4: Change in ThT fluorescence yield with increasing concentration of fibrils. The yield of ThT fluorescence is equal to the ratio $\frac{\text{Fluorescence intensity}}{\text{[insoluble protein]}}$, where the fluorescence intensity and [insoluble protein] values correspond to those measured at the plateau phase of the seeded experiments described in Figure 2a. The data shown in panel a and b correspond to the kinetic traces shown in Figure 2a (left) and Figure 2a (middle and right), respectively.

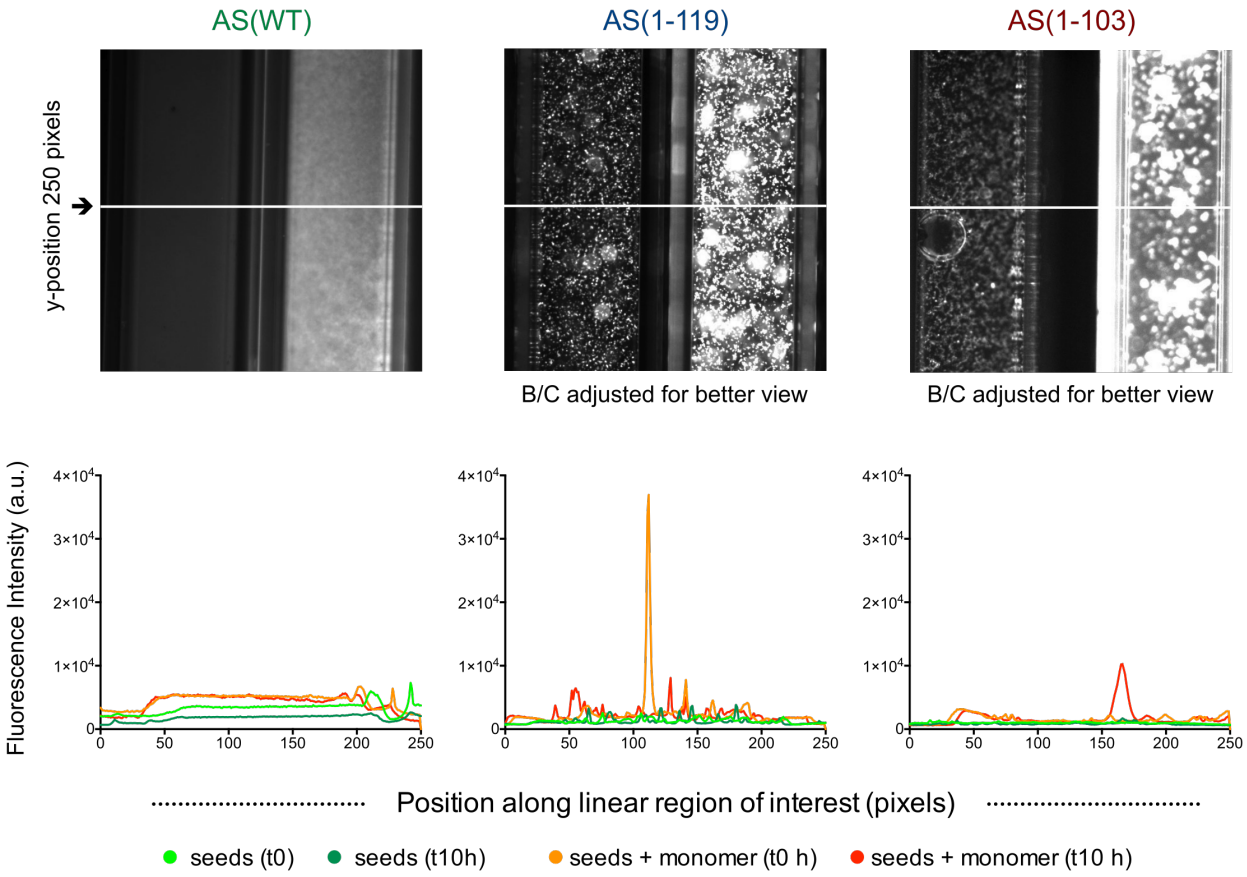

Figure S5: Aggregation of AS(WT), AS(1-119) and AS(1-103) in glass micro-capillaries. Top: Same images as those shown in Figure 3 but with brightness/contrast adjusted to better show details of the fluorescence distribution more clearly. Bottom: Change in the ThT fluorescence along the width of the capillaries at a given y position when fibril seeds where incubated alone (t = 0 (green), t = 10h (dark green)) or in the presence of monomers (t = 0 (orange), t = 10h (red)).

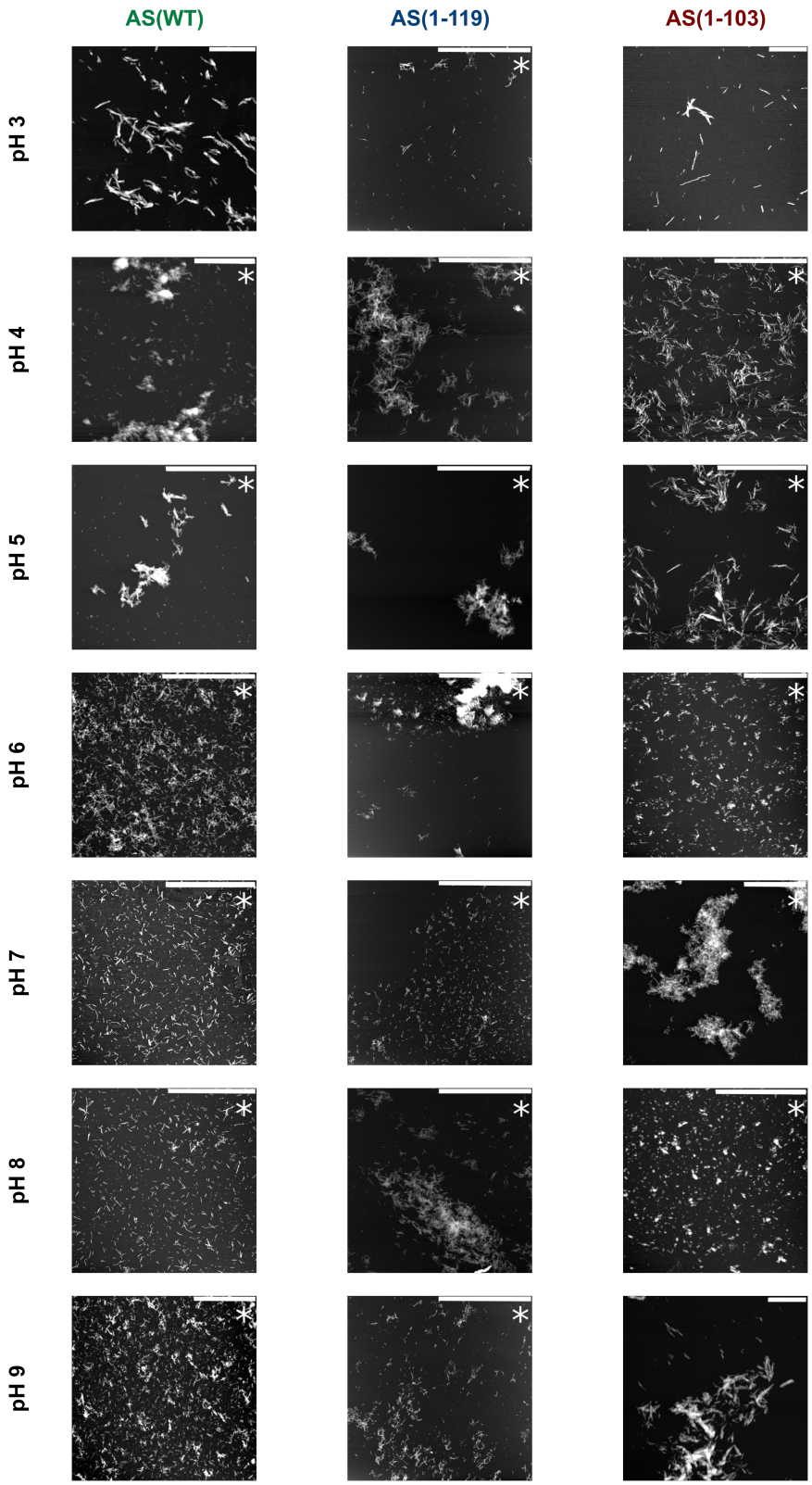

Figure S6: AFM images of amyloid fibrils formed by AS(WT), AS(1-119), AS(1-103) at pH ranging from 3 to 9. Scale bar: 1 μm, scale bar*: 5 μm.

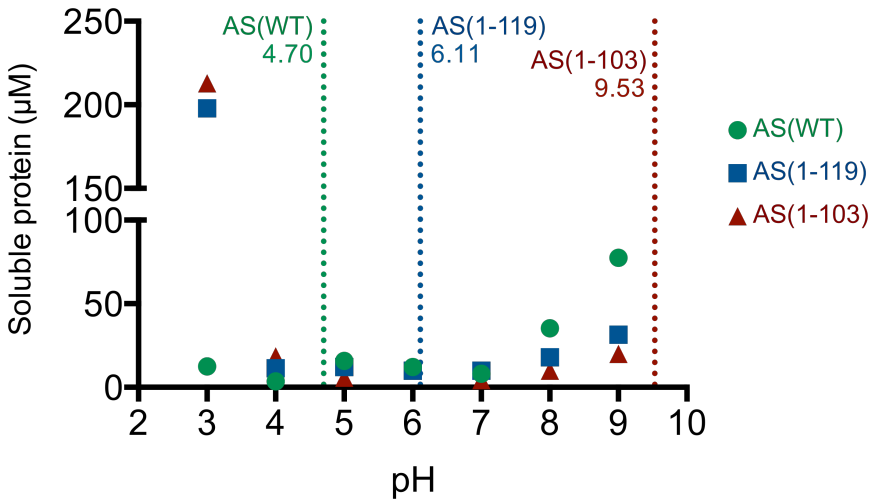

Figure S7: Concentration of soluble protein at the end of fibril formation for AS(WT), AS(1-119) and AS(1-103) as a function of solution pH. Dashed lines are shown at the estimated pI of the three variants.

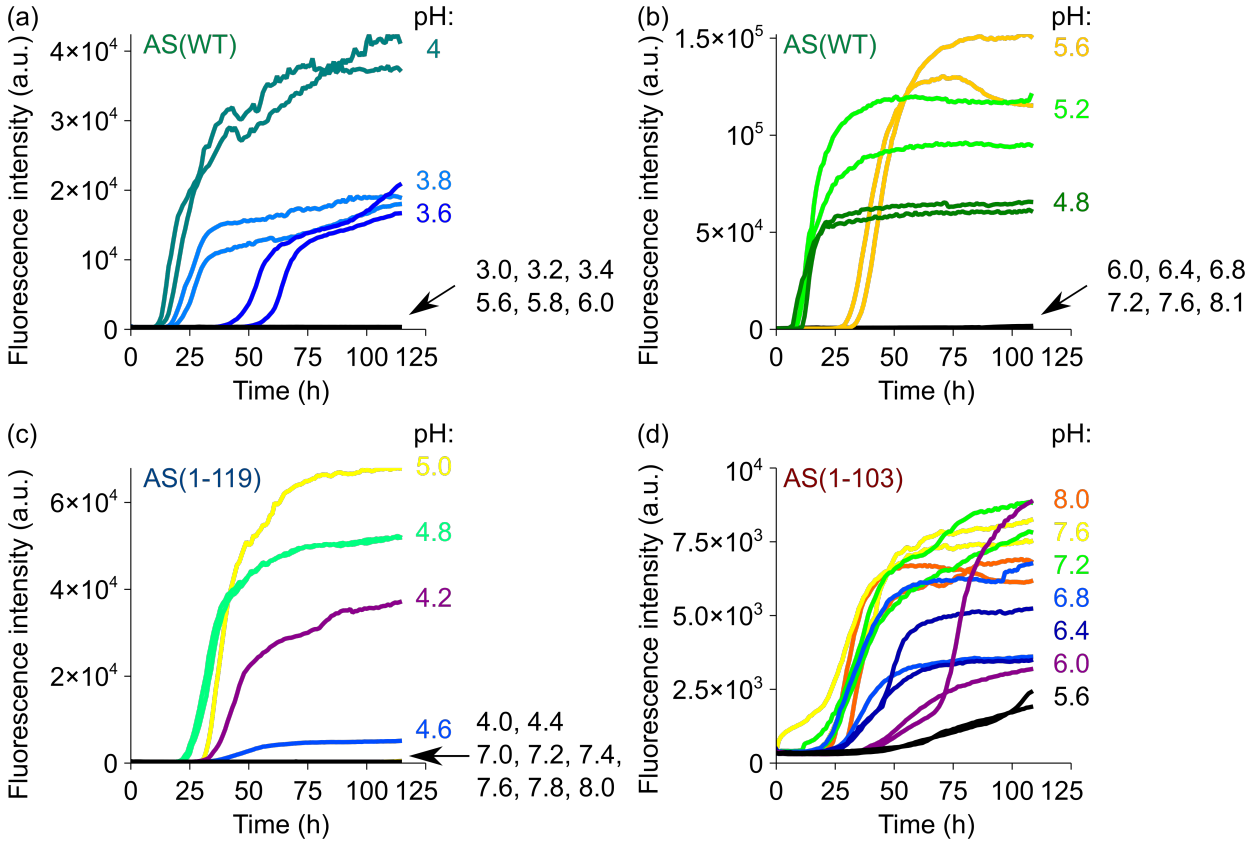

Figure S8: Aggregation of AS(WT), AS(1-119) and AS(1-103) in polystyrene plates at different pH. 10 μM monomeric AS(WT) (a,b), AS(1-119) (c) and AS(1-103) (d) was incubated in polystyrene plates (using 20 μM ThT) in 20 mM sodium phosphate at the indicated pH, at 37°C and quiescent conditions.

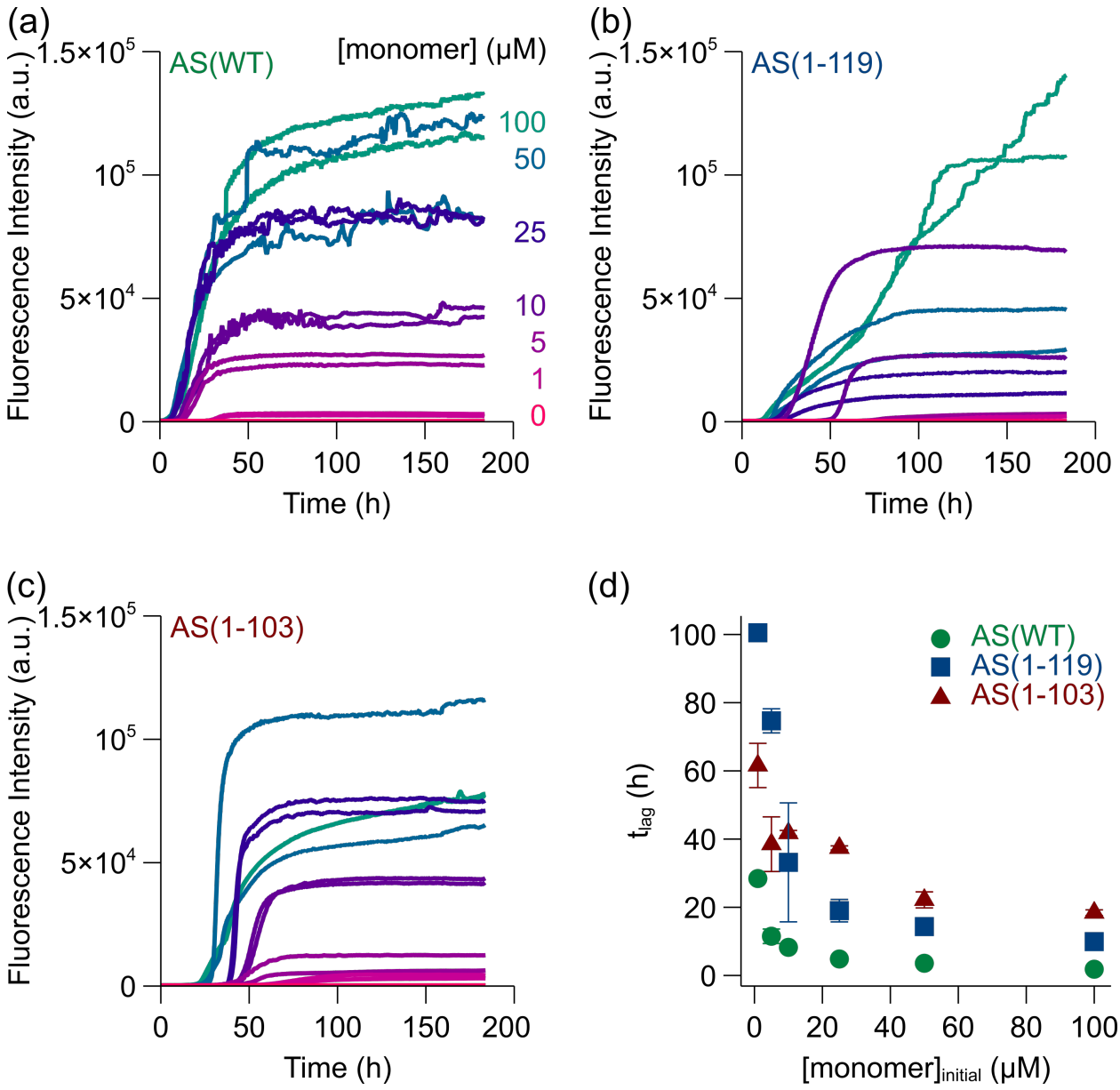

Figure S9: Concentration dependence of the aggregation rate of AS(WT), AS(1-119) and AS(1-103) under conditions where the aggregation is dominated by secondary nucleation. (a-c) Change in the ThT fluorescence when increasing concentrations of monomeric AS(WT) (a), AS(1-119) (b) and AS(1-103) (c) were incubated in polystyrene plates at pH 5, 6 and 7, respectively, at 37°C and under quiescent conditions. (d) Length of the lag phase of the aggregation reactions shown in panels a-c (mean + st. dev., n=2).

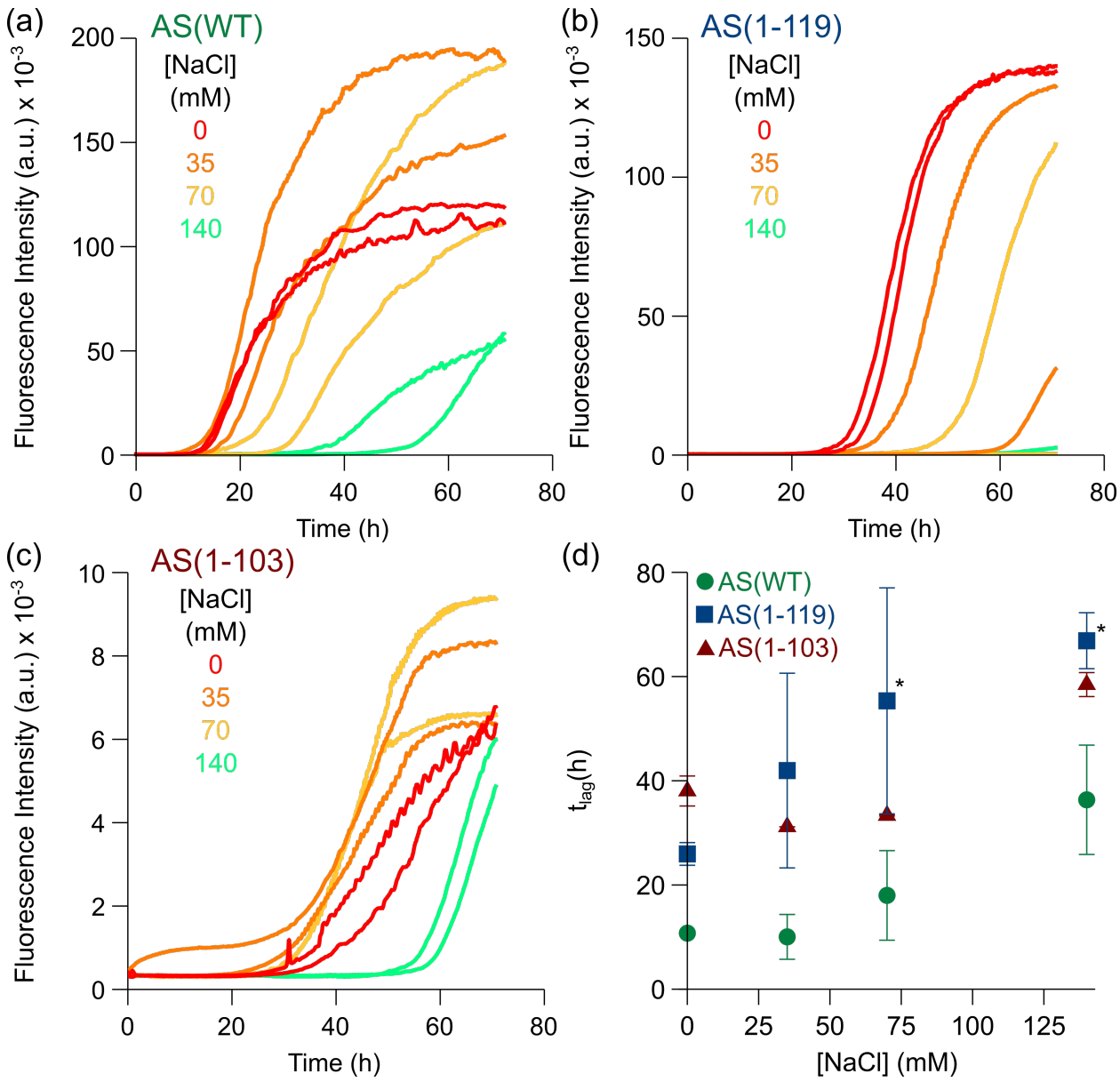

Figure S10: Effect of changes in the ionic strength on the aggregation rate of AS(WT), AS(1-119) and AS(1-103) under conditions where the aggregation is dominated by secondary nucleation. (a-c) Change in the ThT fluorescence when 10 μM AS(WT) (a), AS(1-119) (b) and AS(1-103) (c) were incubated in polystyrene plates at pH 5, 6 and 7, respectively, at 37°C and under quiescent conditions, in the presence of [NaCl] ranging from 0 to 140 mM. (d) Length of the lag phase of the aggregation reactions shown in panels a-c (mean + st. dev., n=2). t_{lag} corresponds to the time at which the fluorescence signal reaches a value greater than 1000 a.u. For the data points marked with an asterisk (*), we took 70h as an upper bound of t_{lag} as the corresponding reaction did not start within the time scale of our measurement.

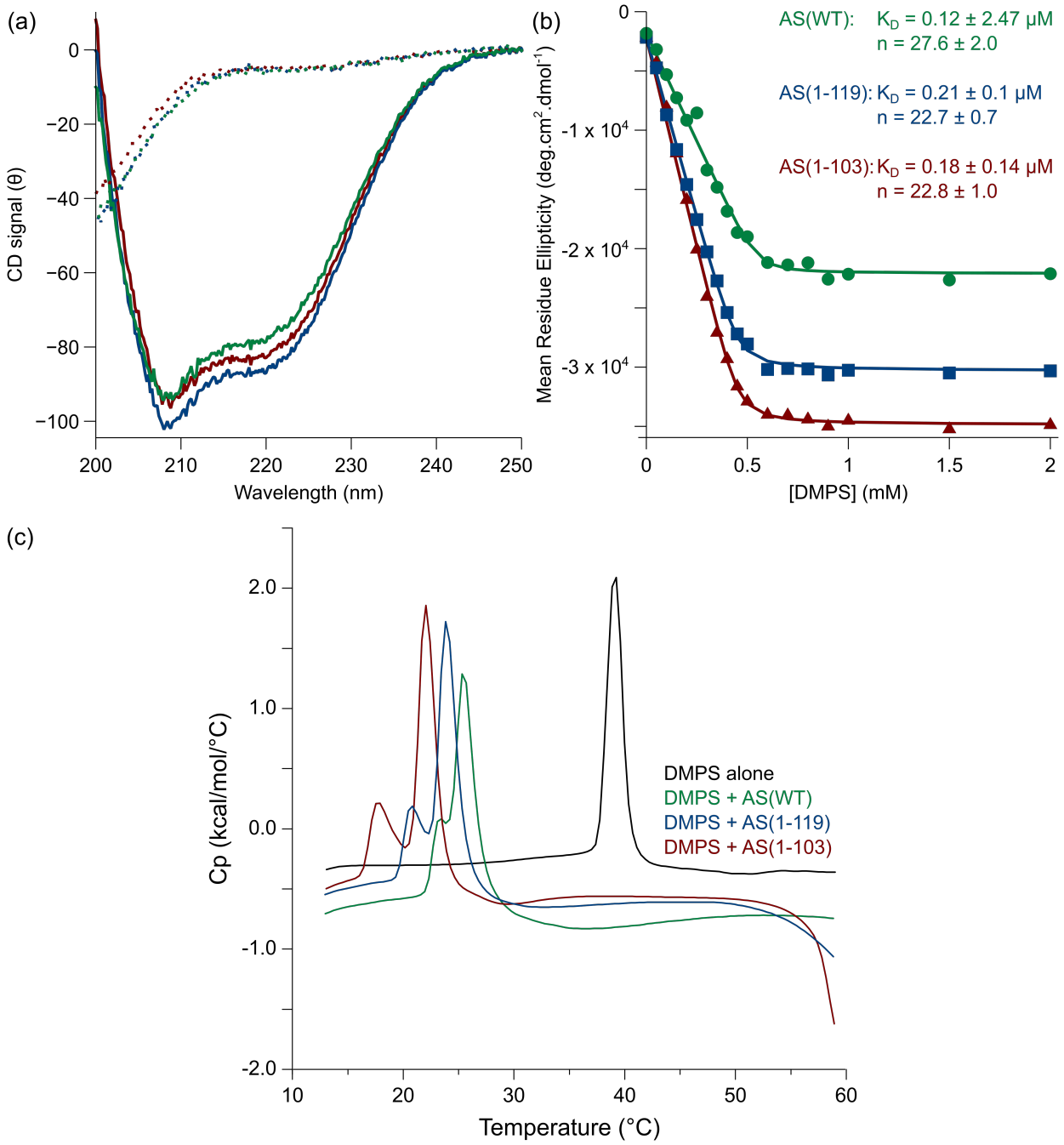

Figure S11: Binding of AS(WT), AS(1-119) and AS(1-103) to DMPS vesicles. (a) CD spectra of 20 μM AS(WT) (green), AS(1-119) (blue) and AS(1-103) (red) in the presence of 0 (bright shades) or 8 mM (dark shades) DMPS at 30 °C. (b) Mean Residue Ellipticity measured at 222 nm when 20 μM AS(WT) (green), AS(1-119) (blue) or AS(1-103) (red) was incubated in the presence of increasing concentration of DMPS (filled symbols). The data were well described by a Langmuir Isotherm[S4] (coloured line) and the corresponding binding constant and stoichiometry are indicated. (c) Thermotropic properties of DMPS bound to AS(WT), AS(1-119) and AS(1-103). DSC thermograms of DMPS (1000 μM) measured in the absence and presence of 100 μM AS(WT), AS(1-119), AS(1-103) in 20mM phosphate buffer pH 6.5.

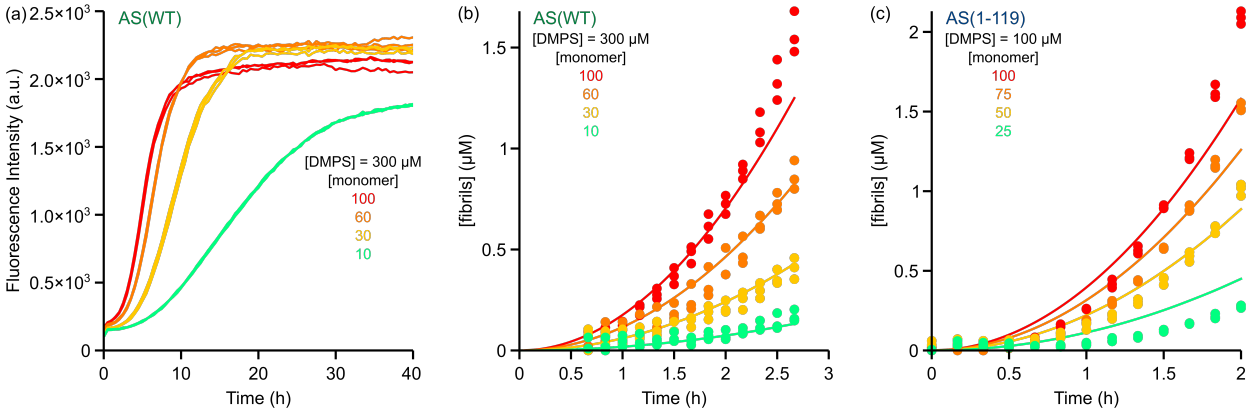

Figure S12: Global analysis of AS(WT) and AS(1-119) lipid-induced aggregation data using a one-step nucleation model. (a-c) Change in ThT fluorescence intensity when increasing concentrations AS(WT) (a,b) or AS(1-119) (c) were incubated in the presence of 100 (c) or 300 μM (a-b) DMPS under quiescent conditions at pH 6.5 and 30°C. (b,c) Global fitting of the early times of the aggregation curves to a one-step nucleation model leads to the determination of the product $k_n k_+$ (3.01 ± 0.04 x 10^{-4} for AS(WT) and 2.10 ± 0.03 x 10^{-3} for AS(1-119) $mol^{-1.2}.s^{-2}$). K_M and n were fixed at 125 μM and 0.2.[S4] The mean squared errors were: 4.53 x 10^{-15} for AS(WT) and 1.27 x 10^{-14} for AS(1-119) μM^2. The data set in panel c corresponds to the measurements performed in Figure 6a.

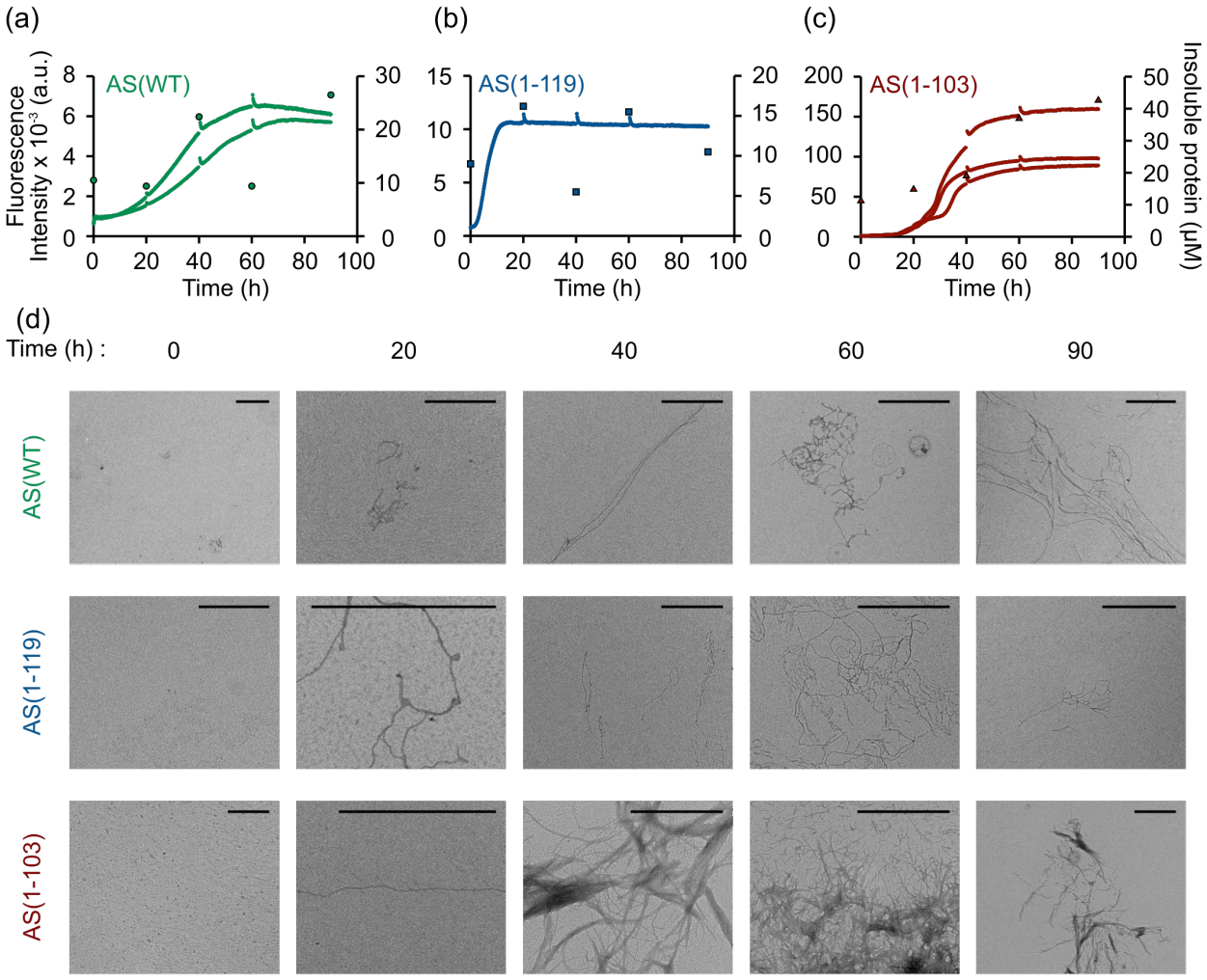

Figure S13: Characterisation of the fibrils formed by AS(WT), AS(1-119) and AS(1-103) during the time course of the lipid-induced aggregation using EM. (a) Change in the ThT fluorescence (left axis, continuous line) and of the concentration of insoluble protein (right axis, individual data points) when 50 μM monomeric AS(WT) (a), AS(1-119) (b) and AS(1-103) (c) were incubated in the presence of 300 μM DMPS vesicles at 30 °C under quiescent conditions. (d) TEM images of samples taken at the different time points displayed in panels a-c, scale bar: 1 μm. Note: the samples used for the TEM imaging did not contain ThT.

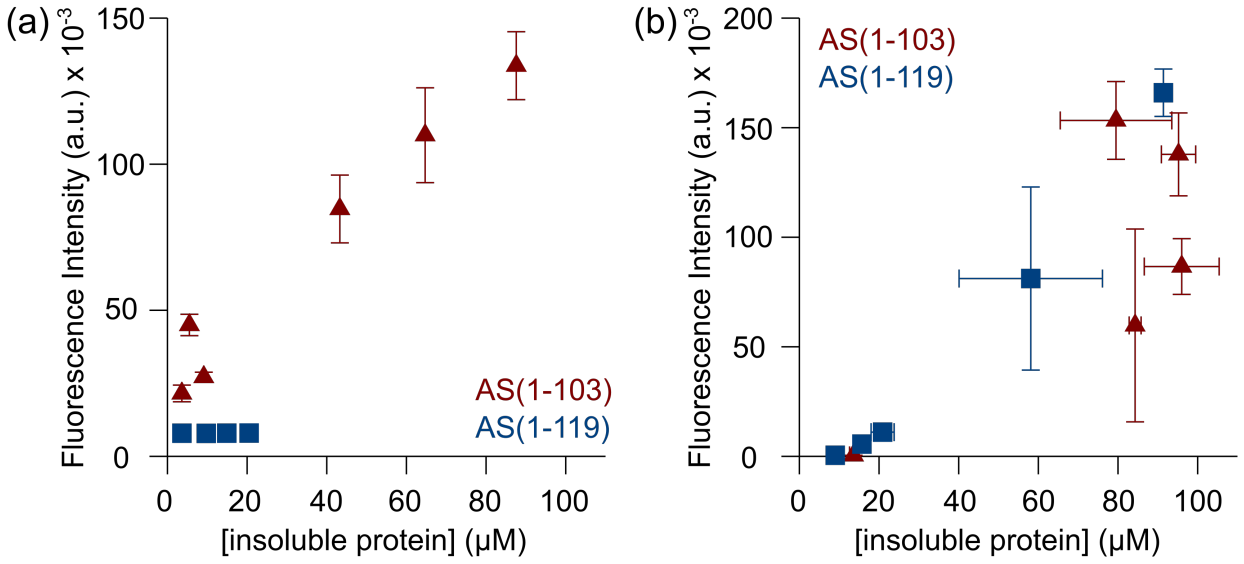

Figure S14: Change in the ThT fluorescence intensity of the lipid-induced aggregation of AS(1-103) and AS(1-119) as a function of the concentration of insoluble protein measured at the plateau phase. The data set in panel a and b correspond to the measurements performed in Figure 6a,b and d,e, respectively.

References

(S1) Grey, M.; Linse, S.; Nilsson, H.; Brundin, P.; Sparr, E. *Journal of Parkinson's Disease* **2011**, *1*, 359–71.

(S2) Hoyer, W.; Antony, T.; Cherny, D.; Heim, G.; Jovin, T. M.; Subramaniam, V. *Journal of Molecular Biology* **2002**, *322*, 383–393.

(S3) Gaspar, R.; Meisl, G.; Buell, A. K.; Young, L.; Kaminski, C. F.; Knowles, T. P. J.; Sparr, E.; Linse, S. *Quarterly Reviews of Biophysics* **2017**, *50*.

(S4) Galvagnion, C.; Buell, A. K.; Meisl, G.; Michaels, T. C. T.; Vendruscolo, M.; Knowles, T. P. J.; Dobson, C. M. *Nature Chemical Biology* **2015**, *11*, 229–234.

(S5) Buell, A. K.; Galvagnion, C.; Gaspar, R.; Sparr, E.; Vendruscolo, M.; Knowles, T. P. J.; Linse, S.; Dobson, C. M. *Proceedings of the National Academy of Sciences of the United States of America* **2014**, *111*, 7671–7676.

(S6) Buell, A. K.; Blundell, J. R.; Dobson, C. M.; Welland, M. E.; Terentjev, E. M.; Knowles, T. P. J. *Physical Review Letters* **2010**, *104*, 228101.

(S7) Baldwin, A. J.; Knowles, T. P. J.; Tartaglia, G. G.; Fitzpatrick, A. W.; Devlin, G. L.; Shammas, S. L.; Waudby, C. A.; Mossuto, M. F.; Meehan, S.; Gras, S. L.; Christodoulou, J.; Anthony-Cahill, S. J.; Barker, P. D.; Vendruscolo, M.; Dobson, C. M. *Journal of the American Chemical Society* **2011**, *133*, 14160–14163.

(S8) Shammas, S. L.; Knowles, T. P. J.; Baldwin, A. J.; Macphee, C. E.; Welland, M. E.; Dobson, C. M.; Devlin, G. L. *Biophysical Journal* **2011**, *100*, 2783–2791.

(S9) Buell, A. K.; Hung, P.; Salvatella, X.; Welland, M. E.; Dobson, C. M.; Knowles, T. P. J. *Biophysical Journal* **2013**, *104*, 1116–1126.

(S10) Galvagnion, C.; Brown, J. W. P.; Ouberai, M. M.; Flagmeier, P.; Vendruscolo, M.; Buell, A. K.; Sparr, E.; Dobson, C. M. *Proceedings of the National Academy of Sciences of the United States of America* **2016**, *113*, 7065–70.

(S11) Crowther, R. A.; Jakes, R.; Spillantini, M. G.; Goedert, M. *FEBS Letters* **1998**, *436*, 309–312.

(S12) Serpell, L. C.; Berriman, J.; Jakes, R.; Goedert, M.; Crowther, R. A. *Proceedings of the National Academy of Sciences of the United States of America* **2000**, *97*, 4897–4902.

(S13) Murray, I. V. J.; Giasson, B. I.; Quinn, S. M.; Koppaka, V.; Axelsen, P. H.; Ischiropoulos, H.; Trojanowski, J. Q.; Lee, V. M.-Y. *Biochemistry* **2003**, *42*, 8530–40.

(S14) Hoyer, W.; Cherny, D.; Subramaniam, V.; Jovin, T. M. *Biochemistry* **2004**, *43*, 16233–42.

(S15) Li, W.; West, N.; Colla, E.; Pletnikova, O.; Troncoso, J. C.; Marsh, L.; Dawson, T. M.; Jakala, P.; Hartmann, T.; Price, D. L.; Lee, M. K. *Proceedings of the National Academy of Sciences of the United States of America* **2005**, *102*, 2162–7.

(S16) Liu, C.-W.; Giasson, B. I.; Lewis, K. a.; Lee, V. M.; Demartino, G. N.; Thomas, P. J. *Journal of Biological Chemistry* **2005**, *280*, 22670–8.

(S17) Mishizen-Eberz, A. J.; Norris, E. H.; Giasson, B. I.; Hodara, R.; Ischiropoulos, H.; Lee, V. M.-Y.; Trojanowski, J. Q.; Lynch, D. R. *Biochemistry* **2005**, *44*, 7818–29.

(S18) Wakamatsu, M.; Ishii, A.; Iwata, S.; Sakagami, J.; Ukai, Y.; Ono, M.; Kanbe, D.; Muramatsu, S.-i.; Kobayashi, K.; Iwatsubo, T.; Yoshimoto, M. *Neurobiology of Aging* **2008**, *29*, 574–585.

(S19) Zhang, F.; Lin, X.-J.; Ji, L.-N.; Du, H.-N.; Tang, L.; He, J.-H.; Hu, J.; Hu, H.-Y. *Biochemical and Biophysical Research Communications* **2008**, *368*, 388–394.

(S20) Ulusoy, A.; Febbraro, F.; Jensen, P. H.; Kirik, D.; Romero-Ramos, M. *European Journal of Neuroscience* **2010**, *32*, 409–422.

(S21) Levitan, K.; Chereau, D.; Cohen, S. I. A.; Knowles, T. P. J.; Dobson, C. M.; Fink, A. L.; Anderson, J. P.; Goldstein, J. M.; Millhauser, G. L. *Journal of Molecular Biology* **2011**, *411*, 329–333.

(S22) Wang, W.; Nguyen, L. T. T.; Burlak, C.; Chegini, F.; Guo, F.; Chataway, T.; Ju, S.; Fisher, O. S.; Miller, D. W.; Datta, D.; Wu, F.; Wu, C.-X.; Landeru, A.; Wells, J. A.; Cookson, M. R.; Boxer, M. B.; Thomas, C. J.; Gai, W. P.; Ringe, D.; Petsko, G. A.; Hoang, Q. Q. *Proceedings of the National Academy of Sciences of the United States of America* **2016**, *113*, 9587–9592.

(S23) Casey, J. R.; Grinstein, S.; Orlowski, J. *Nature Reviews Molecular Cell Biology* **2009**, *11*, 50.